
Article:
Supsrisunjai, C, Hsu, C-K, Michael, M et al. (16 more authors) (2020) Coagulation Factor XIII-A Subunit Missense Mutation in the Pathobiology of Autosomal Dominant Multiple Dermatofibromas. The Journal of Investigative Dermatology, 140 (3). pp. 624-635. ISSN 0022-202X

https://doi.org/10.1016/j.jid.2019.08.441

JID-2019-0484.R1

Coagulation Factor XIII-A Subunit Missense Mutation in the Pathobiology of Autosomal Dominant Multiple Dermatofibromas

Chavalit Supsrisunjai[1,2], Chao-Kai Hsu[1,3,4], Magdalene Michael[5], Cédric Duval[6], John Y. W. Lee[1], Hsing-San Yang[3], Hsin-Yu Huang[7], Thitiwat Chaikul[1], Alexandros Onoufriadis[1], Roberto A. Steiner[5], Robert A. S. Ariëns[6], Ofer Sarig[8], Eli Sprecher[8,9], Marina Schwartz-Eskin[8], Curt Samlaska[10], Michael A. Simpson[11], Eduardo Calonje[1,12], Maddy Parsons[5*], John A. McGrath[1*]

ORCIDs

Chavalit Supsrisunjai: https://orcid.org/0000-0002-1054-6918

Chao-Kai Hsu: https://orcid.org/0000-0003-4365-4533

Magdalene Michael: https://orcid.org/0000-0003-2577-729X

Cédric Duval: https://orcid.org/0000-0002-4870-6542

John Y. W. Lee: https://orcid.org/0000-0002-5563-2334

Hsing-San Yang: https://orcid.org/0000-0002-3973-2896

Hsin-Yu Huang: https://orcid.org/0000-0003-0220-3509

Thitiwat Chaikul: https://orcid.org/0000-0001-5463-3864

Alexandros Onoufriadis: https://orcid.org/0000-0001-5026-0431

Roberto Steiner: https://orcid.org/0000-0001-7084-9745

Robert A. S. Ariëns: https://orcid.org/0000-0002-6310-5745

Ofer Sarig: https://orcid.org/0000-0003-2987-2091

Eli Sprecher: https://orcid.org/0000-0003-0666-0045

Marina Schwartz-Eskin: https://orcid.org/0000-0003-0507-1505

Curt Samlaska: https://orcid.org/0000-0001-7562-4254

Michael A. Simpson: https://orcid.org/0000-0002-8539-8753

Eduardo Calonje : https://orcid.org/0000-0001-7475-6423

Maddy Parsons: https://orcid.org/0000-0002-2021-8379

John A. McGrath: https://orcid.org/0000-0002-3708-9964

[1]St John's Institute of Dermatology, School of Basic and Medical Biosciences, King's College London, Guy's Hospital, London, UK

[2]Institute of Dermatology, Ministry of Public Health, Bangkok, Thailand

[3]Department of Dermatology, National Cheng Kung University Hospital, College of Medicine, National Cheng Kung University, Tainan, Taiwan

[4]International Center for Wound Repair and Regeneration, National Cheng Kung University, Tainan, Taiwan

[5]Randall Centre for Cell and Molecular Biophysics, School of Basic and Medical Biosciences, King's College London, UK

[6]Leeds Institute of Cardiovascular and Metabolic Medicine, University of Leeds, Leeds, UK

[7]School of Medicine, College of Medicine, National Cheng Kung University, Tainan, Taiwan

[8]Division of Dermatology, Tel Aviv Sourasky Medical Center, Tel Aviv, Israel

[9]Department of Human Molecular Genetics & Biochemistry, Sackler Faculty of Medicine, Tel-Aviv University, Tel-Aviv, Israel

[10]Academic Dermatology of Nevada, University of Nevada School of Medicine, Reno, Nevada

[11]Department of Genetics, School of Basic and Medical Biosciences, King's College London, Guy's Hospital, London, UK

[12]Department of Dermatopathology, St John's Institute of Dermatology, Guy's and St Thomas' NHS Foundation Trust, London SE1 9RT, UK

* Joint senior authors. Correspondence should be addressed to JAM (john.mcgrath@kcl.ac.uk)

Corresponding author: John McGrath, Dermatology Research Labs, Floor 9 Tower Wing, Guy's Hospital, Great Maze Pond, London SE1 9RT, United Kingdom. Tel: 44-2071886409; Fax: 44-2071888050; E-mail: john.mcgrath@kcl.ac.uk

Short title: *F13A1* mutation causes familial dermatofibroma

Abbreviations used:

Å angstrom

Akt acutely transforming retrovirus AKT8 in rodent T cell lymphoma

CDM cell-derived matrix

Col I collagen type I

ERK extracellular signal–regulated kinase

ExAC Exome Aggregation Consortium

FBS fetal bovine serum

FN fibronectin

FXIII-A Factor XIII subunit A

GAPDH glyceraldehyde-3-phosphate dehydrogenase

GFP green fluorescent protein

GST glutathione S-Transferase

GTP guanosine triphosphate

HEK human embryonic kidney

HET heterozygous

HRP horseradish peroxidase

ILDT Isoleucine-Leucine-Aspartate-Threonine

IRES internal ribosome entry site

MAPK mitogen-activated protein kinase

NHDF normal human dermal fibroblast

PBS phosphate buffered saline

PDGF platelet-derived growth factor

PDGFR platelet-derived growth factor receptor

Pl3K phosphatidylinositol 3 kinase

TBS Tris buffered saline

WES whole exome sequencing

WT wild type

Abstract

Dermatofibromas are common benign skin lesions, the etiology of which is poorly understood. We identified two unrelated pedigrees in which there was autosomal dominant transmission of multiple dermatofibromas. Whole exome sequencing revealed a rare shared heterozygous missense variant in *F13A1* gene encoding factor XIII subunit A, a transglutaminase involved in hemostasis, wound healing, tumor growth, and apoptosis. The variant (p.Lys679Met) has an allele frequency of 0.0002 and is predicted to be a damaging mutation. Recombinant human Lys679Met FXIII-A demonstrated reduced fibrin crosslinking activity *in vitro*. Of note, treatment of fibroblasts with media containing Lys679Met FXIII-A led to enhanced adhesion, proliferation and type I collagen synthesis. Immunostaining revealed co-localization between FXIII-A and α4β1 integrins, more prominently for Lys679Met FXIII-A than wild-type. In addition, both the α4β1 inhibitors and the mutation of the FXIII-A Isoleucine-Leucine-Aspartate-Threonine (ILDT) motif prevented Lys679Met FXIII-A-dependent proliferation and collagen synthesis of fibroblasts. Our data suggest that the Lys679Met mutation may leads to a conformational change in the FXIII-A protein that enhances α4-integrin binding and provide insight into an unexpected role for FXIII-A in the pathobiology of familial dermatofibroma.

INTRODUCTION

Dermatofibromas are common benign fibro-histiocytic tumors (Jakobiec et al., 2014; 2017). Typically, dermatofibromas present as solitary 0.5-1cm pink, red, tan or flesh-colored lumps with an overlying dimple-like depression (Zelger and Zelger, 1998). Sometimes multiple dermatofibromas may occur, occasionally in families, but more often in individuals with underlying immunologic or other clinical abnormalities (Beatrous et al., 2017). The most common site for dermatofibromas is the lower legs, with usual onset during early adulthood. The cause of dermatofibromas is not known although dermatologists may suggest they occur following insect bites in susceptible individuals, or possibly following trauma (Kluger et al., 2008; Myers and Fillman 2019).

Histologically, in dermatofibromas (single or multiple) there are interlacing fascicles of slender spindle-shaped cells within a loose collagenous, or occasionally myxoid, stroma. Of note, hemosiderin is frequently present. Immunohistochemically, almost all dermatofibromas are FXIII-A (factor XIIIA antigen)-positive (Altman et al., 1993), and indeed immunostaining for FXIII-A is frequently used in the tissue diagnosis of dermatofibromas (Cerio et al., 1988; 1989).

In this study, we performed whole exome sequencing (WES) to identify the causative mutation in two seemingly unrelated pedigrees with autosomal dominant familial multiple dermatofibromas. Intriguingly, we identified the same mutation in *F13A1* encoding the A-subunit of factor XIII (FXIII-A) in both families. FXIII is a member of transglutaminase family which crosslinks various proteins involved in hemostasis, wound healing, tumor growth, and apoptosis (Muszbek et al., 2011). During wound healing, FXIII modulates fibroblast and macrophage biology and contributes to angiogenesis (Bagoly et al., 2012, Duval et al., 2016, Muszbek et al., 2011). While plasma FXIII is composed of two catalytic A subunits and two

non-catalytic carrier B units generating a A_2B_2 heterotetramer (Komaromi et al., 2011), cellular FXIII (found, for example, in platelets and megakaryocytes) is formed solely of A subunits organized in an A_2 homodimer. The mutation we identified in this study affects the A subunit, i.e. it impacts on both the plasma and tissue/cellular FXIII forms (PMID: 30489000, PMID: 5096097). We provide evidence that the FXIII-A mutation leads to enhanced proliferation and collagen synthesis in fibroblasts, potentially through promoting binding of exogenous FXIII-A to integrins. Our study therefore provides insight into an important role for FXIII-A in the etiology and pathobiology of some dermatofibromas.

RESULTS

Clinical features and histology

We examined seven affected individuals from two unrelated families with multiple dermatofibromas inherited in an autosomal dominant pattern (Figure 1a). Three affected individuals were from the Ukraine (Family 1) and four affected were from the USA (Family 2). Both families were Jewish (Ashkenazi). Some clinicopathologic details of Family 2 have been published previously (Samlaska and Bennion, 2002). All subjects presented with multiple lesions of erythematous papules over extremities (Figure 1b; illustrations from Family 1 and 2) with histopathologic findings of dermatofibromas (Figure 1c; Family 1, II-2). No extra-cutaneous manifestations were reported.

All individuals with multiple dermatofibromas are heterozygous for the mutation c.2036A>T (Lys679Met) in *F13A1*

We undertook WES in six affected subjects from the Ukraine and US families and two unaffected individuals from the US family. Candidate mutations were prioritized by filtering for variants with a frequency of less than 0.01% in public repositories such as the 1000 Genomes Project, Exome Aggregation Consortium (ExAC) and an in-house database (Supplementary Table S1, S2). Using these criteria, a missense variant in *F13A1* encoding Factor XIII subunit A (c.2036A>T; rs201302247) was the only variant present in all affected individuals in both families. Subsequent Sanger sequencing confirmed the mutation in affected individuals (Supplementary Figure S1) and co-segregated with disease status in all relatives who provided DNA samples. This variant was rare in the population (less than 0.0207% frequency) and resulted in an amino acid change from lysine to methionine at position 679 (position 678 in the mature protein) with an *in silico* prediction that the mutation is damaging (Polyphen-2 = 1; Mutation taster = 1; CADD = 25.5; DANN = 0.993).

c.2036A>T in *F13A1* is a rare allele found most commonly in Ashkenazi Jews

To investigate the possibility that c.2036A>T was inherited from a common ancestor, we performed a haplotype analysis to study the mutant alleles from affected individuals using four highly polymorphic single nucleotides polymorphism markers based on the exome data (Supplementary Figure S2). The data showed identical haplotypes among affected individuals (in contrast to the unaffected individuals) indicating that c.2036A>T probably occurred on the same ancestral allele. Of note, the allele frequency of rs201302247 in Ashkenazi Jews (0.397%) is almost 20 times higher than that in the general population (Genome Aggregation Database; https://gnomad.broadinstitute.org/variant/6-6152055-T-A). The incidence of familial multiple dermatofibromas is not known (in any population) but our data indicate that, although rare and perhaps underreported, it may be substantially higher in Ashkenazi Jews.

Mutations in *F13A1* are not detectable in sporadic dermatofibromas

To explore whether mutations in *F13A1* might also be present in the more common sporadic dermatofibromas, we undertook Sanger sequencing of the coding and promoter regions of *F13A1* using DNA extracted from paraffin-embedded tissue of 22 sporadic single dermatofibromas from unrelated individuals; no potentially deleterious variants were identified (Supplementary Methods and Results, and Tables S3-S6).

The mutation Lys679Met in FXIII-A results in reduced crosslinking activity

To assess the activity of the Lys679Met mutant FXIII-A protein, we generated Glutathione S-Transferase (GST)-fusions of wild-type (WT) or Lys679Met FXIII-A (see Supplementary Table S7 for site directed mutagenesis details), purified recombinant proteins (Figure 2a) and performed pentylamine incorporation into casein assays. We found that the Lys679Met FXIII-A mutation led to reduced crosslinking at 30 min by 50% compared to WT protein (Figure 2b, c). To find possible clues for the altered catalytic activity we looked at the available structural information. Factor XIII-A is composed of five major structural regions: an N-terminal activation peptide (residues 1-38), a β-sandwich domain (residues 39-184), a catalytic domain (185-516), and two β-barrel domains (517-628 and 629-732) that in the inactive FXIII-A zymogen are arranged in a dimer (Figure 2d) (Yee et al., 1994; Weiss et al., 1998). Residue Lys679 is solvent exposed and maps on a β-strand of the second β-barrel domain. In the inactive enzyme, access to active site is occluded by an intramolecular interaction within the first β-barrel domain which, in turn, is stabilized by the N-terminal peptide of the second FXIII-A molecule. Enzyme activation involves thrombin cleavage of the activation peptide in the presence of Ca^{2+} ions, and calcium binding results in dimer destabilization and a large structural

rearrangement involving a swinging movement of both β-barrel domains (Figure 2e). This leads to an active FXIII-A monomer in which the active site is accessible (Stieler et al., 2013). In the active conformation observed by crystallography, Lys679 is located away from the active site (more than 63 angstroms (Å)) ruling out a direct effect of the Lys to Met mutation on the catalytic machinery. This mutation could alternatively play a role in the activation mechanism. The first five amino acids of the activation peptide are not visible in the structure of the inactive FXIII-A dimer and Lys679 is approximately 22 Å away from the first ordered residue (Arg 6). Thus, based on distance considerations, stabilization of the flexible N-terminal peptide by the Lys679Met residue would require some structural rearrangements. We should also point out that in our pentylamine incorporation assay we employed Prescission-cleaved recombinant FXIII-A. Therefore, we cannot exclude that the slightly longer N-terminus resulting from the cloning strategy fortuitously might be stabilized by the Lys679Met mutation more than occurs *in vivo* wherein the Ser2 is expected to be acetylated following cleavage of the first methionine (GPMSETSR…. instead of Ac-SETSR….). More detailed biochemical experiments need to be performed to validate the observed change in catalytic activity and understand its possible molecular basis.

The mutation Lys679Met in FXIII-A promotes proliferation and collagen production in human dermal fibroblasts

Proliferation assays were performed to determine whether FXIII-A contributes to fibroblast cell proliferation in dermatofibromas. To expose fibroblasts to FXIII-A, we expressed WT or Lys679Met FXIII-A coupled to GFP by means of an IRES in human embryonic kidney (HEK293) cells and collected secreted protein in the conditioned media. Both WT and Lys679Met constructs yielded similar levels of secreted protein (Figure 3a, inset blot).

Treatment of fibroblasts with this media demonstrated that incubation with WT FXIII-A led to higher proliferation rates after 48h, whereas Lys679Met FXIII-A led to significantly higher proliferation rates at both 24 and 48h post-incubation (Figure 3a). To determine whether treatment with FXIII-A also altered pro-fibrotic matrix secretion by fibroblasts, collagen I and fibronectin levels were assessed in whole cell lysates. Western blots revealed a significant increase in collagen synthesis in Lys679Met FXIII-A treated cells but not those treated with WT FXIII-A media, compared to controls (Figure 3b), whereas no change in levels of fibronectin were detected between samples (Supplementary Figure S3a). Quantitative PCR analysis further demonstrated upregulation of collagen I mRNA levels in Lys679Met FXIII-A treated cells compared to WT (Figure 3c). To further analyze native ECM deposition by cells, fibroblasts were grown for 14 days on coverslips to generate cell-derived matrix (CDM) in the presence or absence of FXIII-A. Imaging of the resulting CDM preparations revealed an apparent increase in disorganized collagen production in cells treated with Lys679Met FXIII-A compared to WT (Figure 3d). These combined data suggest that FXIII-A can promote fibroproliferative responses in fibroblasts and that the identified Lys679Met mutation enhances this property of FXIII-A.

Lys679Met FXIII-A shows higher association with α4β1 integrins on fibroblasts

Our data demonstrated that, in contrast to lower activity as a coagulation factor, Lys679Met FXIII-A exhibited more activity in terms of a fibroproliferation. Previous data have suggested that FXIII-A binds to α4β1 integrin to elicit some cellular activities (Isobe et al., 1999). To explore this possibility, we performed early adhesion assays to collagen I substrates of fibroblasts pre-treated with WT or Lys679Met FXIII-A. Data revealed a significant increase in adhesion of cells treated with Lys679Met FXIII-A compared to WT or control samples (Figure

3e), suggesting enhanced integrin activation in these cells. Given that α4β1 integrin is a fibronectin receptor and does not directly bind to collagen I, other matrix receptors e.g. α1β1, α2β1 integrin may be involved in the binding.

To investigate whether FXIII-A binds to specific sites on the cell surface, the localization patterns of FXIII-A, α4 and active β1 integrins were analyzed in FXIII-A-treated fibroblasts by confocal microscopy. Images and subsequent analysis revealed that active β1 integrins co-localized with WT FXIII-A and this was significantly increased for Lys679Met FXIII-A (Figure 4a, b). Moreover, levels of active β1 integrins were significantly higher in Lys679Met FXIII-A treated cells compared to WT or untreated cells (Figure 4c), further supporting the notion that mutant FXIII-A can activate integrin receptors at the surface of fibroblasts. Similarly, α4 integrins showed a significant increase in co-localization between with Lys679Met FXIII-A compared to WT (Figure 4d, e), indicating that mutant FXIII-A either binds with higher specificity to α4 integrin, or that the protein remains at these sites for longer after binding. No significant difference in levels of total α4 integrin protein were observed between WT and Lys679Met FXIII-A treated cells, (Supplementary Figure S3c, d) suggesting that FXIII-A exerts effects at the level of integrin localization in fibroblasts. This observation suggests FXIII-A associates with integrins and results in increased receptor activation.

To further investigate whether FXIII-A may co-operate with α4β1 to elicit phenotypic effects, cells were pre-treated with α4β1-specific inhibitors (BIO1211, BOP and TCS2134) prior to treatment with FXIII-A. Confocal imaging of α4β1 integrins revealed a visible reduction in the levels of both WT and Lys679Met FXIII-A associated with the plasma membrane in cells treated with BIO1211, suggesting active α4β1 is required for FXIII-A binding to the plasma membrane (Figure 5a). Further analysis demonstrated that all three integrin inhibitors suppressed the Lys679Met FXIII-A-dependent increase in collagen

synthesis (Figure 5b) and proliferation (Figure 5c). These observations suggest that FXIII-A requires α4 integrin to associate with the membrane and promote fibroproliferative responses.

FXIII-A has previously been suggested to associate with integrins through the isoleucine-leucine-aspartate-threonine 'ILDT' amino acid motif located on the catalytic domain (Isobe et al., 1999). To test this hypothesis, site-directed mutagenesis was performed to mutate the ILDT motif to AAAA in FXIII-A and define the potential role of this site in regulating fibro-proliferative phenotypes. We found that mutation of ILDT to AAAA resulted in inhibition of the FXIII-A-induced increase in both collagen production and proliferation (Figure 5d, e). These data support the notion that FXIII-A can bind to α4 through the ILDT motif and that this region may co-operate with the residues around Lys679 to promote α4 association.

FXIII-A regulates mitogen-activated protein kinase (MAPK) and phosphatidylinositol 3 kinase (PI3K) activation

To further investigate potential mechanisms by which FXIII-A promotes cell proliferation and collagen synthesis, we analyzed activation of a range of different signaling pathways in cells treated with WT or Lys679Met FXIII-A. Tissue transglutaminase has been reported to promote platelet-derived growth factor receptor (PDGFR)-integrin association, and we therefore hypothesized that FXIII-A binding may enhance activation of this pathway (Zemskov et al., 2009). Western blotting analysis of cells treated with WT or Lys679Met FXIII-A revealed no significant increase in PDGFR activity (as judged by pTyr-751 reactivity, Figure 6a). There were also no detectable changes in activity of the small guanosine triphosphatase (GTPase) RhoA, that is known to be activated downstream of integrins and can contribute to collagen synthesis (Supplementary Figure S3e). However, further analysis of other downstream

signaling targets (Akt, ERK1/2, p38alpha) revealed that pAkt and pERK both showed significantly increased activation levels in cells following 1h of treatment with both WT and Lys679Met FXIII-A (Figure 6a, b, c). Taken together, these data suggest that FXIII-A can promote activation of Akt and MAPK pathways, which may potentially increase cell proliferation (Figure 6d).

DISCUSSION

Dermatofibroma is a common benign fibro-histiocytic skin tumor but little is known about its pathogenesis (Hsi and Nickoloff, 1996). Typically, dermatofibromas are thought to be induced by trauma, particularly following insect bites. Here, we investigated two unrelated pedigrees with autosomal dominant familial multiple dermatofibromas and identified a heterozygous missense mutation in FXIII-A. On one level this is a surprising finding given that FXIII-A antibodies have been used for the last 40 years for the immunohistochemical diagnosis of dermatofibromas (Cerio et al., 1988). Nevertheless, we also demonstrated that the mutant FXIII-A protein has a functional impact with reduced crosslinking activity but increased fibroblast cell proliferation and adhesion and type I collagen synthesis. Thus, FXIII-A is not only a useful immunohistochemical marker for dermatofibromas but it is also directly implicated in the molecular genetics of families with multiple dermatofibromas, at least in this study.

FXIII-A is found mainly in macrophages and other cell types including fibroblast-like mesenchymal cells and is expressed in many fibrovascular tumors (Cerio et al., 1989, Nemeth and Penneys, 1989). Indeed, in dermatofibromas, aside from fibroblasts, the main cellular component comprises cells of monocyte/macrophage lineage and it is these cells that mainly express FXIII-A. In addition, FXIII-A is also present in platelet granules (Muszbek et al.,

2011). Our working hypothesis, therefore, is that an insect bite or direct trauma may promote a bleed (hemosiderin is common in dermatofibromas, Figure 1c lower image). This bleeding may be enhanced by the presence of Lys679Met FXIII-A which shows reducing clot stabilization function (but no clinical bleeding abnormality). The small bleed then triggers platelet plug formation, platelet granule degradation and release of FXIII-A that then impacts on fibroblast cell biology and collagen production. Still to be explored and currently unexplained, however, is the role of mutant FXIII-A in monocyte/macrophages.

Previously, autosomal recessive mutations in FXIII-A (mostly A-subunit, rarely B) have been identified in very rare bleeding disorders (incidence ~1 in 5 million), sometimes with wound healing abnormalities (Karimi et al., 2009), but no pathogenic autosomal dominant mutations have been previously described. The mutation Lys679Met is not a novel variant but is present in the general population with low frequency (risk allele frequency 0.0207%; rs201302247); the allele is more common among Ashkenazi Jews (Genome Aggregation Database). Our expectation is that other individuals with this heterozygous missense mutation may also have multiple dermatofibromas, although this remains to be proven. Regarding sporadic, non-familial dermatofibromas, we did not find any evidence for *F13A1* genetic variants and therefore the role that FXIII-A may play (or not) in such lesions awaits further study.

Previous reports have suggested that recessive mutations within the β-barrel 1 and β-barrel 2 domains of FXIII-A can affect the regions of the protein that regulate conformational changes during activation (Thomas et al., 2016). Our analysis suggests that the Lys679Met mutation is more likely to have an impact on the activation step rather than a direct effect on the catalytic machinery. The exact molecular details of how this might occur are not yet clear.

Two key phenotypes of dermatofibroma are fibroblast proliferation and collagen production. In contrast to reduced coagulation function, the mutation Lys679Met clearly enhances both pro-fibrotic and proliferative effects, as evidenced by the proliferation data and type I collagen qPCR, western blots and cell-derived matrix production. Our data also suggest that FXIII-A associates with α4β1integrins at the plasma membrane to elicit these phenotypic effects and that this is mediated via the ILDT motif in FXIII-A. Lys679Met FXIII-A may bind with a higher affinity or for a greater length of time to α4 integrins. However, biochemical *in vitro* studies to assess direct binding would be required to validate this hypothesis.

We further explored the link between α4 integrin activation and proliferation and collagen synthesis. Published evidence suggests that upon activation, integrins can activate PDGFR or LRP-6 (Muramatsu et al., 2004, Ren et al., 2013, Zemskov et al., 2009) although we did not observe any activation in these receptors. We also did not observe changes to the activity of RhoA upon FXIII-A addition to fibroblasts. We demonstrated significant increases in pERK1/2 and pAkt upon FXIII-A binding, which are key downstream targets in the RAS/RAF/MEK/ERK and the PI3K/Akt signaling pathways, but there were no differences between WT and Lys679Met (De Luca et al., 2012). For now, we conclude that the proposed enhanced action of Lys679Met FXIII-A on α4 integrin could initiate different signaling cascades which remain to be determined (Figure 6d).

In summary, our study provides insight into the genetic and cellular basis of a subset of familial dermatofibromas and highlight an extended role for FXIII-A in their pathobiology.

MATERIALS AND METHODS

Whole Exome Sequencing (WES) and Sanger Sequencing

Following informed consent from the patients and ethics committee approval, WES was performed using DNA from available probands and their family members by the Illumina HiSeq2500 system (Illumina, San Diego, CA). The Exome capture kit (Agilent SureSelect Human All Exon 50 Mb kit, Santa Clara, CA) was used to prepare DNA libraries from 3 µg of DNA. First, the Adapted Focused Acoustic technology (Covaris, Woburn, MA) was used to shear genomic DNA to yield a mean of 150bp fragment size. The fragment ends were then repaired, ligated with sequencing adaptors and hybridized against biotinylated 120bp RNA probes (Agilent) targeting protein-coding genomic regions for 24 hours. Targeted regions were selected for with magnetic streptavidin-coated beads while unbound DNA was washed off. The exome-enriched DNA pool was next eluted, amplified with low-cycle PCR, multiplexed (4 samples on each lane) and sequenced with 100bp paired-end reads. Reads were aligned to the GRCh37/hg19 reference genome using Novoalign (Novocraft Technologies, Selangor, Malaysia). The Bedtools package and custom scripts were used to calculate the depth of sequence coverage (Quinlan and Hall, 2010). The SAMtools software was used for variant calling and quality filtering (Li et al., 2009). Variants were then annotated with multiple passes through the ANNOVAR software package (Wang et al., 2010). PCR and Sanger sequencing were performed to validate the segregation of the mutation with phenotypes according to standard protocol using primers for *F13A1* exon14 (Supplementary Tables S5).

Purification of FXIII-A- GST fusion proteins for functional analysis

pGEX-FXIII-A, an expression vector encoding an N-terminal GST-FXIII-A fusion protein, was generated as previously described (Smith et al., 2011). Lys679Met FXIII-A variant was generated by site-directed mutagenesis using the listed primers (Supplementary Table S7) with QuickChange II Kit (Agilent Technologies; Stockport, UK). Successful mutagenesis was

verified by DNA sequencing. Both FXIII-A plasmids were then transformed into XL10-Gold® Ultra-competent *E. Coli* (Agilent Technologies, Wokingham, UK). FXIII-A_2 Expression and purification were performed as previously described (Duval et al., 2016).

FXIII-A activity analysis by Pentylamine Incorporation

Measurement of FXIII activity was performed using a modified 5-(biotinamido) pentylamine incorporation assay. Nunc-Immuno- 96 Micro-Well plates were coated with 100µl of 10µg/ml N, N-dimethylated casein overnight at 4°C, then blocked with 300µl 1% BSA in Tris buffer saline (TBS) for 90min at 37°C. Plates were then washed with 4x 300µl TBS and 10µl of samples (WT or Lys679Met rhFXIII-A_2 or murine plasma) were added to the wells in triplicate. 90µl of activation mix (111µM dithiothreitol, 0.3µM biotinylated pentylamine, 11mM $CaCl_2$, 2.2U/ml thrombin) was added and the reactions were stopped at 0, 20, 40, 60, 80, 100, 120 min by adding 200µl of 200mM EDTA. Plates were washed with 4x 300µl 0.1% [v/v] Tween20 in TBS, and 100µl of 2µg/ml of streptavidin in 1% [w/v] BSA (in TBS-Tween) were added for 60min at 37°C. Following washes with 4x 300µl TBS-Tween, 100µl of 1mg/ml phosphatase substrate (in 1M diethanolamine) were added, and the reaction was stopped by adding 100µl of 4M NaOH. Absorbency was measured at 405nm, using a SpectraMax 190 absorbance microtiter plate reader (Molecular Devices, Wokingham, UK). The rate of pentylamine incorporation over time was then used as an indicator of PreScission-cleaved FXIII activity. Experiments were performed in triplicate.

Normal human dermal fibroblast (NHDF) and HEK293 cell culture

NHDFs (Cellworks, Buckingham, UK) up to passage number 10 and HEK293 cell (ATCC; Middlesex, UK) were cultured in DMEM in high glucose (4.5g/L), 10 % (v/v) fetal bovine

serum (FBS), 50µg/ml penicillin and 2mM L-glutamine in a humidified incubator at 37°C with 5%CO_2. Cells were tested for Mycoplasma infection with Mycoalert™ Mycoplasma Detection Kit (Lonza, Slough, UK).

Plasmids constructs, site directed mutagenesis and FXIII-A expression in HEK293 cell line

Site-directed mutagenesis was performed on the mammalian expression vector pIRES2-EGFP expression vector containing the cDNA FXIII-A (a kind gift from Consuelo González-Manchón, Madrid; Jayo et al., 2009) according to the QuikChange Lightning Site-Directed Mutagenesis Kit protocol (Agilent Technologies) using primers (Supplementary Table S7). Transient transfection was performed using Lipofectamine 3000 on HEK293 Cell line. Transfected cells were grown in 2% FBS containing media for 48 hours before collecting the conditioned media for experiments. FXIII-A expression level was verified by Western blotting.

Proliferation, adhesion assays and cell-derived matrix (CDM) preparation

Fibroblasts were plated in media containing 2% serum a day before the experiment. Cells then were treated with conditioned media containing either WT or Lys679Met FXIII-A for 24 and 48 hours for proliferation assay. Collagen type I solution from rat tail (Sigma-Aldrich) at a concentration of 50µg/ml was used to coat a plate for adhesion assays. For CDM preparation, cells were grown on 0.2% crosslinked gelatin-coated coverslips for 14 days before cell denudation, as previously described (Kaukonen et al., 2017). Cells and matrices were then fixed for 10 minutes at room temperature with 4% final concentration of paraformaldehyde. Cells were permeabilized with 0.1% Triton-X100 in phosphate buffered saline (PBS) solution for 10 minutes followed by 1-hour incubation with 3% BSA in PBS solution containing 1:400

phalloidin-AlexaFluor488 and 1:1000 DAPI. The images of cells were acquired by tile-scans of each well using EVOSTM FL Auto 2 Imaging System (ThermoFisher, Waltham, MA) with a 10x objective lens. The number of cells in each well was measured by automated nuclei counting using ImageJ.

Reverse Transcription PCR

Fibroblasts were treated with WT and Lys679Met FXIII-A for 48 hours. Total RNA was extracted using RNeasy Micro Kit (Qiagen). The quality of RNA was analyzed by the Nanodrop spectrophotometer (ThermoFisher). Reverse Transcription was performed using High-Capacity cDNA Reverse Transcription Kit according to the manufacturer's protocol. Gene expression was assessed by real-time PCR by using TagMan® Gene Expression Assays for *Col1a1* Mm00801666_g1 (ThermoFisher). Transcript levels were normalized to GAPDH expression, measured with Applied Biosystems (Foster City, CA) TaqMan probes.

Western blot analysis

Whole-cell lysates of fibroblasts were collected after treatment with FXIII-A conditioned media using RIPA buffer with protease inhibitor cocktail set I (Calbiochem, San Diego, CA). Each sample was resuspended in NuPAGE™ LDS Sample Buffer (Invitrogen™), boiled at 100°C for 5 minutes and run on NuPAGE™ 4-12% Bis-Tris Protein Gels (Invitrogen™). Resolved proteins were transferred and blotted onto nitrocellulose membrane. Primary and secondary antibodies are listed (Supplementary Table S8).

Immunofluorescence and confocal microscopy

Fibroblasts on coverslips were treated with WT and Lys679Met FXIII-A over variable time points, then washed and fixed with 4% paraformaldehyde in PBS before 10-minute permeabilization with 0.1% Triton-X100, followed by blocking with 5% BSA in PBS for 30 minutes. Cells were labelled with antibodies (Supplementary Table S8) at 4°C overnight and then stained with secondary antibodies (Supplementary Table S8), phalloidin-AlexaFluor568 and DAPI. Cells were imaged with 60x objective using Nikon A1R inverted confocal microscope. Images were exported from Nikon Elements software for further analysis in ImageJ software using intensity functions of the co-localization analysis plugin JaCoP.

Data Availability Statement

Datasets related to this article can be found at https://www.ncbi.nlm.nih.gov/bioproject/PRJNA545215, hosted at Sequence Read Archive (SRA) under the collection ID PRJNA545215.

Conflict of Interest

The authors have no conflicts of interest to declare.

Acknowledgements

The authors acknowledge financial support from Rosetrees Trust, Medical Research Council UK (MR/M018512/1) and the National Institute for Health Research (NIHR) Biomedical Research Centre based at Guy's and St Thomas' NHS Foundation Trust, King's College London, U.K and Department of Medical Services, Ministry of Public Health, Thailand.

CRediT statement

Conceptualization, C.S., M.P. and J.A.M. Investigation, C.S., C.K.H., M.M., C.D., J.Y.W.L., T.C., R.S., R.A.S.A and M.P. Formal Analysis, C.S. C.K.H, C.D., T.C., A.O., M.A.S., J.E.C and M.P. Methodology, C.S., C.K.H., M.P. Resources, H-S.Y., H-Y. H., O.S., E.S., M.S-E, Cu.S. Supervision, M.P., J.A.M. Writing, original draft, C.S. Writing, review & editing, C.S., M.P. and J.A.M.

REFERENCES

Altman DA, Nickoloff BJ, Fivenson DP. Differential expression of factor XIIIa and CD34 in cutaneous mesenchymal tumors. J Cutan Pathol 1993;20:154-8.

Bagoly Z, Katona E, Muszbek L. Factor XIII and inflammatory cells. Thromb Res 2012;129 Suppl 2:S77-81.

Beatrous SV, Riahi RR, Grisoli SB, Cohen PR. Associated conditions in patients with multiple dermatofibromas: Case reports and literature review. Dermatol Online J 2017;23.

Cerio R, Griffiths CE, Cooper KD, Nickoloff BJ, Headington JT. Characterization of factor XIIIa positive dermal dendritic cells in normal and inflamed skin. Br J Dermatol 1989;121:421-31.

Cerio R, Spaull J, Jones EW. Identification of factor XIIIa in cutaneous tissue. Histopathology 1988;13:362-4.

De Luca A, Maiello MR, D'Alessio A, Pergameno M, Normanno N. The RAS/RAF/MEK/ERK and the PI3K/AKT signalling pathways: role in cancer pathogenesis and implications for therapeutic approaches. Expert Opin Ther Targets 2012;16 Suppl 2:S17-27.

Duval C, Ali M, Chaudhry WW, Ridger VC, Ariens RA, Philippou H. Factor XIII A-Subunit V34L Variant Affects Thrombus Cross-Linking in a Murine Model of Thrombosis. Arterioscler Thromb Vasc Biol 2016;36:308-16.

Hsi ED, Nickoloff BJ. Dermatofibroma and dermatofibrosarcoma protuberans: an immunohistochemical study reveals distinctive antigenic profiles. J Dermatol Sci 1996;11:1-9.

Isobe T, Takahashi H, Ueki S, Takagi J, Saito Y. Activity-independent cell adhesion to tissue-type transglutaminase is mediated by alpha4beta1 integrin. Eur J Cell Biol 1999;78:876-83.

Jakobiec FA, Rai R, Yoon MK. Fibrous histiocytoma of the tarsus: clinical and immunohistochemical observations with a differential diagnosis. Cornea 2014;33:536-9.

Jakobiec FA, Zakka FR, Tu Y, Freitag SK. Dermatofibroma of the Eyelid: Immunohistochemical Diagnosis. Ophthal Plast Reconstr Surg 2017;33:e134-8.

Jayo A, Conde I, Lastres P, Jimenez-Yuste V, Gonzalez-Manchon C. Possible role for cellular FXIII in monocyte-derived dendritic cell motility. Eur J Cell Biol 2009;88:423-31.

Kaukonen R, Jacquemet G, Hamidi H, Ivaska J. Cell-derived matrices for studying cell proliferation and directional migration in a complex 3D microenvironment. Nat Protoc 2017;12:2376-90.

Karimi M, Bereczky Z, Cohan N, Muszbek L. Factor XIII Deficiency. Semin Thromb Hemost 2009;35:426-38.

Kluger N, Cotten H, Magana C, Pinquier L. Dermatofibroma occurring within a tattoo: report of two cases. J Cutan Pathol 2008;35:696-8.

Komaromi I, Bagoly Z, Muszbek L. Factor XIII: novel structural and functional aspects. J Thromb Haemost 2011;9:9-20.

Li H, Handsaker B, Wysoker A, Fennell T, Ruan J, Homer N, et al. The Sequence Alignment/Map format and SAMtools. Bioinformatics 2009;25:2078-9.

Muramatsu H, Zou P, Suzuki H, Oda Y, Chen GY, Sakaguchi N, et al. alpha4beta1- and alpha6beta1-integrins are functional receptors for midkine, a heparin-binding growth factor. J Cell Sci 2004;117:5405-15.

Muszbek L, Bereczky Z, Bagoly Z, Komaromi I, Katona E. Factor XIII: a coagulation factor with multiple plasmatic and cellular functions. Physiol Rev 2011;91:931-72.

Myers DJ, Fillman EP. Dermatofibroma. [Updated 2019 Feb 15]. In: StatPearls [Internet]. Treasure Island (FL): StatPearls Publishing; 2019; Available from: https://www.ncbi.nlm.nih.gov/books/NBK470538/

Nemeth AJ, Penneys NS. Factor XIIIa is expressed by fibroblasts in fibrovascular tumors. J Cutan Pathol 1989;16:266-71.

Quinlan AR, Hall IM. BEDTools: a flexible suite of utilities for comparing genomic features. Bioinformatics 2010;26:841-2.

Ren S, Johnson BG, Kida Y, Ip C, Davidson KC, Lin SL, et al. LRP-6 is a coreceptor for multiple fibrogenic signaling pathways in pericytes and myofibroblasts that are inhibited by DKK-1. Proc Natl Acad Sci U S A 2013;110:1440-5.

Samlaska C, Bennion S. Eruptive dermatofibromas in a kindred. Cutis 2002; 69:187-8,190.

Smith KA, Adamson PJ, Pease RJ, Brown JM, Balmforth AJ, Cordell PA, et al. Interactions between factor XIII and the alpha C region of fibrinogen. Blood 2011;117:3460-8.

Stieler M, Weber J, Hils M, Kolb P, Heine A, Büchold C, et al. Structure of active coagulation factor XIII triggered by calcium binding: basis for the design of next-generation anticoagulants. Angew Chem Int Ed Engl 2013;52:11930-4.

Thomas A, Biswas A, Dodt J, Philippou H, Hethershaw E, Ensikat HJ, et al. Coagulation factor XIIIA subunit missense mutations affect structure andf at the various steps of factor XIII action. Hum Mutat 2016;37:1030-41.

Wang K, Li M, Hakonarson H. ANNOVAR: functional annotation of genetic variants from high-throughput sequencing data. Nucleic Acids Res 2010;38:e164.

Weiss MS, Metzner HJ, Hilgenfeld R. Two non-proline cis peptide bonds may be important for factor XIII function. FEBS Lett. 1998;423:291-6.

Yee VC, Pedersen LC, Le Trong I, Bishop PD, Stenkamp RE, Teller DC. Three-dimensional structure of a transglutaminase: human blood coagulation factor XIII. Proc Natl Acad Sci U S A. 1994;91:7296-300.

Zelger BG, Zelger B. Dermatofibroma. A clinico-pathologic classification scheme. Pathologe 1998;19:412-9.

Zemskov EA, Loukinova E, Mikhailenko I, Coleman RA, Strickland DK, Belkin AM. Regulation of platelet-derived growth factor receptor function by integrin-associated cell surface transglutaminase. J Biol Chem 2009;284:16693-703.

Figure legends:

Figure 1: Clinicopathologic and molecular basis of familial multiple dermatofibromas. (**a**) Pedigrees of the two families showing all affected individuals with the *F13A1* mutation c.2036A>T (Lys679Met). (**b**) Multiple dermatofibromas in Family 1 individual II-2 (left) and Family 2 individuals II-3 (right). (**c**) Histopathologic features of an excised dermatofibromas from an individual II-2 in Family 1 showing proliferation of fibro-histiocytic cells within the dermis with an overlying Grenz zone (left image; hematoxylin and eosin, ×4; scale bar 500μm

). There is collagen entrapment at the periphery of the lesion as well as presence of hemosiderin pigment (right image; hematoxylin and eosin, ×10; scale bar 200μm).

Figure 2: Mutation Lys679Met in FXIII-A leads to reduced protein activity (**a**) SDS PAGE gel showing purity and levels of WT and Lys679Met FXIII-A purified recombinant proteins used in the assay. (**b**) Graph showing rate of pentylamine incorporation over time in preparations containing WT or Lys679Met mutant protein. (**c**) Percentage biotin incorporation as an estimation of FXIII activity. The data display means +/- SD for three experiments. *** = p=0.0007. (**d**) Cartoon representation of the inactive FXIII-A dimer (PDB code 1F13). For one FXIII-A molecule distinct structural regions are labeled and highlighted using different colors. The second FXIII-A molecule is shown in grey. Residue Lys679 is shown as stick representation in black. Residues of the catalytic triad are shown in orange. Lys679 is located ~22 Å away from the first ordered residue of the N-terminal activation peptide. (**e**) Cartoon representation of Ca2+-activated FXIII-A monomer (PDB code 4KTY) shown in the same orientation as in (d) Color-codes for the distinct structural regions are the same as in (d). The inhibitor bound in the active site is shown in cyan. Calcium ions are shown as grey spheres. Residue Lys679 is shown as stick representation in black. Ca2+-induced activation elicits a large swinging movement of the β-barrel domains. In this conformation Lys679 is located ~63 Å away from the active site.

Figure 3: Mutation Lys679Met in FXIII-A leads to increased fibroblast proliferation, collagen production and changes in extracellular matrix organization. (**a**) Graph shows that NHDF proliferation is increased for Lys679Met FXIII-A compared to WT FXIII-A at both 24 and 48 hours. (**b**) Collagen I western blot and (**c**) qPCR show that Lys679Met FXIII-A

promotes more collagen I production after 48 hours compared to WT FXIII-A. (**d**) Images of CDM produced by cells showing those treated with Lys679Met FXIII-A express more collagen made of thickened fibers compared to WT FXIII-A (scale bars 10um). (**e**) Adhesion assay showing number of cells adhering to collagen I-coated plate at 1 hour is greater for Lys679Met FXIII-A compared to WT FXIII-A. The data indicate means +/- SD for three experiments* = $p<0.05$ * * = $p<0.01$ vs control, *** = $p<0.001$ vs control. All experiments were done in triplicate (n=3). C, W and M indicates control, wild type or mutant, respectively.

Figure 4: Co-localization of α4, β1 and FXIII-A on the cell surface suggests FXIII-A binds to α4β1 integrin Immunofluorescence staining and confocal microscopy of fixed, permeabilized NHDFs on coverslips after treatment with WT FXIII-A or Lys679Met FXIII-A for 2 hours before fixation. (**a**) Images show co-localization of active β1integrin and FXIII-A after treatment with either WT or mutant FXIII-A (scale bars 10um). (**b**) Manders overlap co-efficient analysis showing percentage overlap between FXIII-A and active β1integrin is greater for Lys679Met FXIII-A. (**c**) Level of Active β1 integrin intensity per cell is greater for Lys679Met FXIII-A. (**d**) Images show co-localization of α4 integrin and FXIII-A which is greater for Lys679Met FXIII-A compared to WT FXIII-A (scale bars 10um). (**e**) Manders overlap co-efficient analysis showing percentage overlap between FXIII-A and integrin is greater for Lys679Met FXIII-A. All experiments were done in triplicate. The data represent means +/- SD for three experiments* = $p<0.05$ vs control ** = $p<0.01$ vs control *** = $p<0.001$ vs control

Figure 5: FXIII-A associates with α4β1integrin via the ILDT motif in FXIII-A. (**a**) NHDFs on coverslips were pre-treated with either DMSO (control) or BIO1211 (α4β1 integrin inhibitor) for 2 hours and then WT FXIII-A, Lys679Met FXIII-A and control conditioned

media was added for 1 hour. Confocal images show that BIO1211 induces internalization of α4 integrin (small green dots); there is less FXIII-A binding for both WT and Lys679Met FXIII-A when cells are incubated with BIO1211 (scale bars 10um). (**b**) Western blots show reduction in collagen I expression after incubation with 3 different integrin inhibitors (BIO1211, BOP, TCS2314), particularly for cells treated with Lys679Met FXIII-A compared to WT FXIII-A. (**c**) Graph shows reduced cell proliferation rates following FXIII-A treatment (WT or Lys679Met) compared to control after incubation with the 3 integrin inhibitors at 48 hours. (**d**) Western blot shows reduction of Collagen I expression after 48-hour treatment with ILDT235_238AAAA FXIII-A. (**e**) Graph shows reduced cell proliferation rate after site-directed mutagenesis of ILDT motif of FXIII-A. These effects for (f) and (g) are common to the WT and Lys679Met FXIII-A but are more marked with Lys679Met FXIII-A. Experiments were performed in triplicate. The data show means +/- SD for three experiments*= $p<0.05$ vs control ** = $p<0.01$ vs control ***= $p<0.001$ vs control. C, W and M indicates control, wild type or mutant, respectively.

Figure 6: WT and Lys679Met FXIII-A both increase Akt and ERK1/2 activation. (**a**) NHDFs were treated with FXIII-A for 1, 4, or 8 hours with 2 nM PDGF-BB treatment as a positive control. Activation levels of PDGFR and Akt were determined by immunoblotting with antibodies to Tyr (p)-751-PDGFRβ and Ser(p)-473-Akt1. All samples were normalized for equal amount with glyceraldehyde-3-phosphate dehydrogenase (GAPDH). No activation was noted for p-PDGFR whereas both WT and Lys679Met FXIII-A showed transient increase in p-Akt signaling at 1 hour. (**b**) Activation level of LRP-6, ERK1/2 and p38α were determined by immunoblotting with antibodies to Ser (p)-1490-LRP6, Thr202 (p)/Thr204 (p)-p44/42MAPK (ERK1/2) and Thr (p)-180)/Tyr (p)-182-p38α. All samples were normalized for equal amounts with GAPDH. Both WT and Lys679Met FXIII-A showed transient increase in

p-ERK1/2 signaling at 1 hour. (**c**) Phosphoproteins were quantified, averaged and expressed for NHDF cells treated with WT and Lys679Met FXIII-A as fold change over those of untreated cells. Both WT and Lys679Met FXIII-A showed similar ~two-fold increases in p-Akt and p-ERK1/2 compared to control. Shown are the means +/- SD for three experiments. (**d**) A proposed schematic figure for FXIII-A and α4β1 integrins association on the cell surface and downstream signaling. Lys679Met may lead to a conformational change in the protein which promotes α4 integrin binding (right panel). WT and Lys679Met FXIII-A after association with integrins activate Akt and Erk1/2 resulting in cell proliferation, adhesion and collagen production. However, the enhanced action of mutant FXIII-A on α4 integrin could initiate different signaling cascades which still remain to be determined.

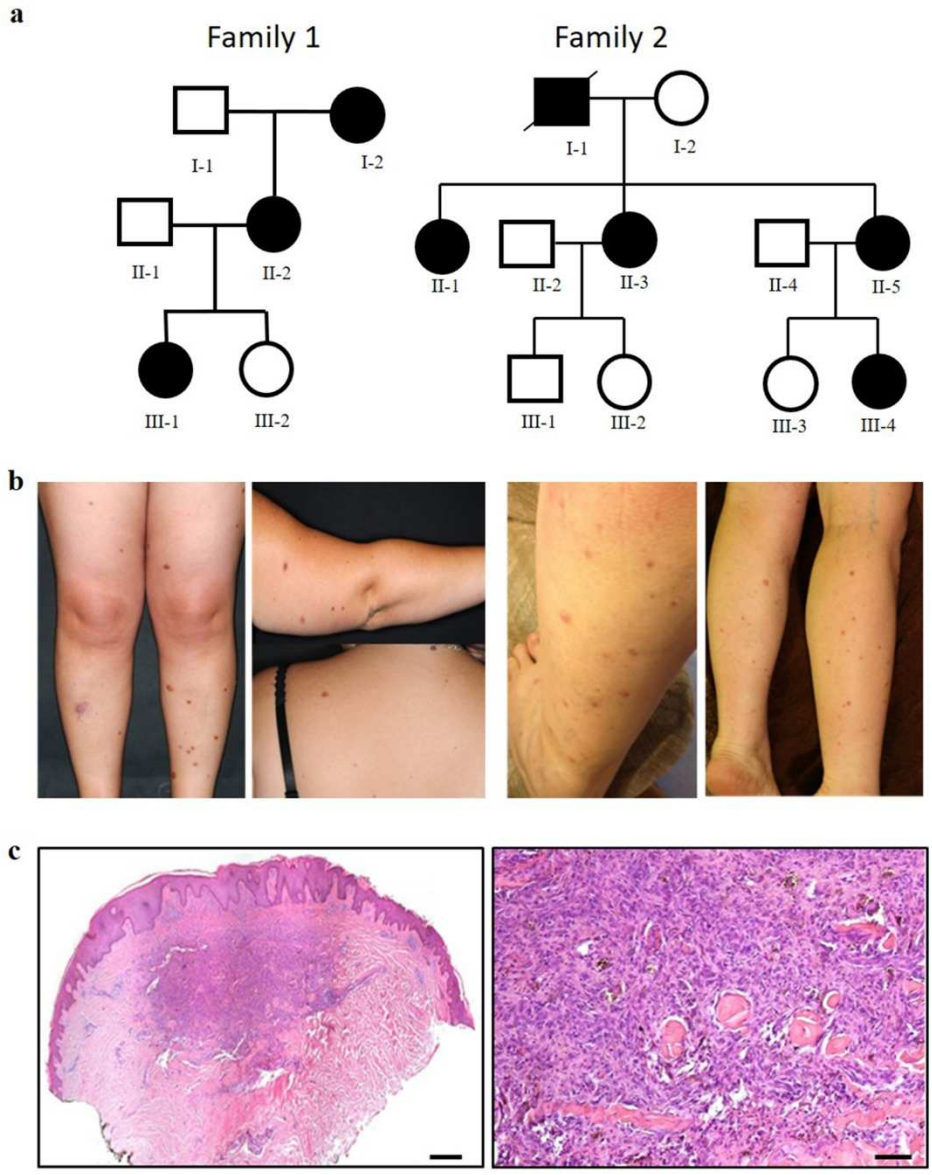

Figure 1: Clinicopathologic and molecular basis of familial multiple dermatofibromas. (a) Pedigrees of the two families showing all affected individuals with the F13A1 mutation c.2036A>T (Lys679Met). (b) Multiple dermatofibromas in Family 1 individual II-2 (left) and Family 2 individuals II-3 (right). (c) Histopathologic features of an excised dermatofibromas from an individual II-2 in Family 1 showing proliferation of fibro-histiocytic cells within the dermis with an overlying Grenz zone (left image; hematoxylin and eosin, ×4; scale bar 500μm). There is collagen entrapment at the periphery of the lesion as well as presence of hemosiderin pigment (right image; hematoxylin and eosin, ×10; scale bar 200μm).

179x221mm (300 x 300 DPI)

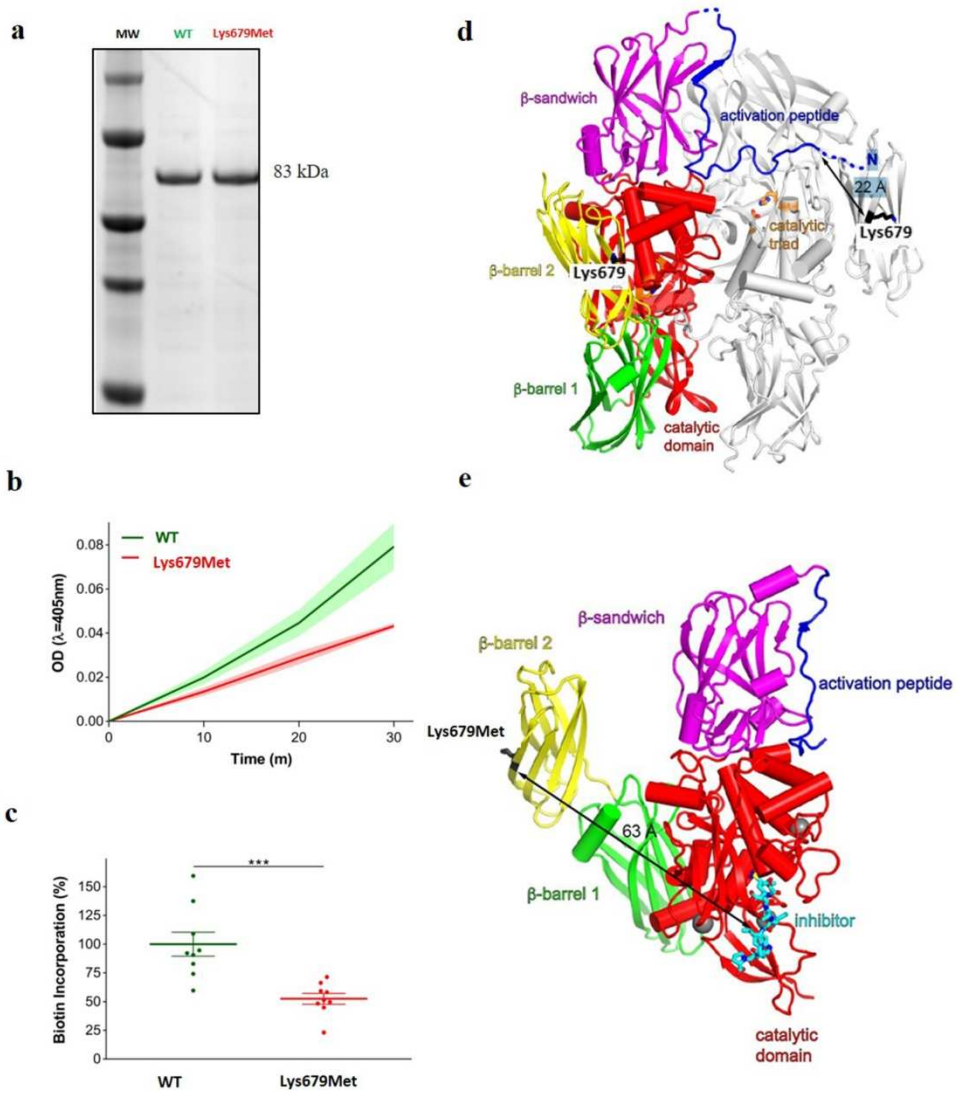

Figure 2: Mutation Lys679Met in FXIII-A leads to reduced protein activity (a) SDS PAGE gel showing purity and levels of WT and Lys679Met FXIII-A purified recombinant proteins used in the assay. (b) Graph showing rate of pentylamine incorporation over time in preparations containing WT or Lys679Met mutant protein. (c) Percentage biotin incorporation as an estimation of FXIII activity. The data display means +/- SD for three experiments. *** = p=0.0007. (d) Cartoon representation of the inactive FXIII-A dimer (PDB code 1F13). For one FXIII-A molecule distinct structural regions are labeled and highlighted using different colors. The second FXIII-A molecule is shown in grey. Residue Lys679 is shown as stick representation in black. Residues of the catalytic triad are shown in orange. Lys679 is located ~22 Å away from the first ordered residue of the N-terminal activation peptide. (e) Cartoon representation of Ca2+-activated FXIII-A monomer (PDB code 4KTY) shown in the same orientation as in (d) Color-codes for the distinct structural regions are the same as in (d). The inhibitor bound in the active site is shown in cyan. Calcium ions are shown as grey spheres. Residue Lys679 is shown as stick representation in black. Ca2+-induced activation elicits a large swinging movement of the β-barre ldomains. In this conformation Lys679 is located ~63 Å away from the active site.

184x212mm (300 x 300 DPI)

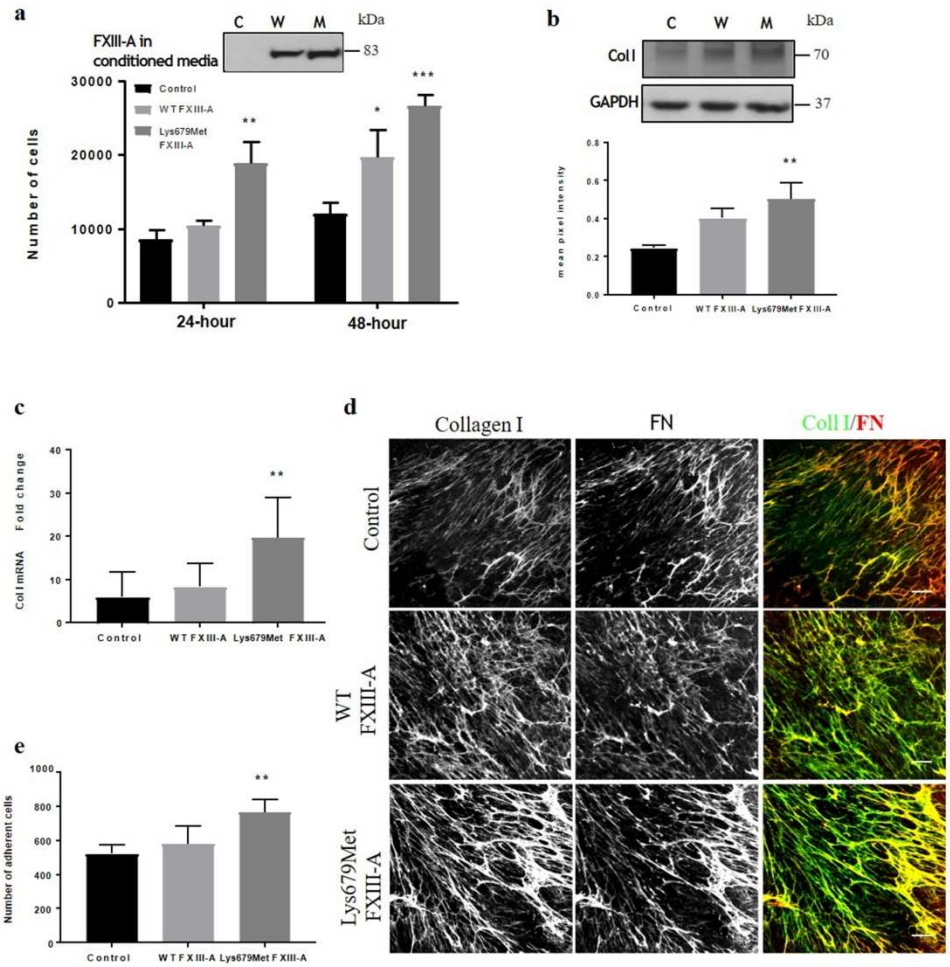

Figure 3: Mutation Lys679Met in FXIII-A leads to increased fibroblast proliferation, collagen production and changes in extracellular matrix organization. (a) Graph shows that NHDF proliferation is increased for Lys679Met FXIII-A compared to WT FXIII-A at both 24 and 48 hours. (b) Collagen I western blot and (c) qPCR show that Lys679Met FXIII-A promotes more collagen I production after 48 hours compared to WT FXIII-A. (d) Images of CDM produced by cells showing those treated with Lys679Met FXIII-A express more collagen made of thickened fibers compared to WT FXIII-A (scale bars 10um). (e) Adhesion assay showing number of cells adhering to collagen I-coated plate at 1 hour is greater for Lys679Met FXIII-A compared to WT FXIII-A. The data indicate means +/- SD for three experiments* = $p<0.05$ * * = $p<0.01$ vs control, *** = $p<0.001$ vs control. All experiments were done in triplicate (n=3). C, W and M indicates control, wild type or mutant, respectively.

198x208mm (300 x 300 DPI)

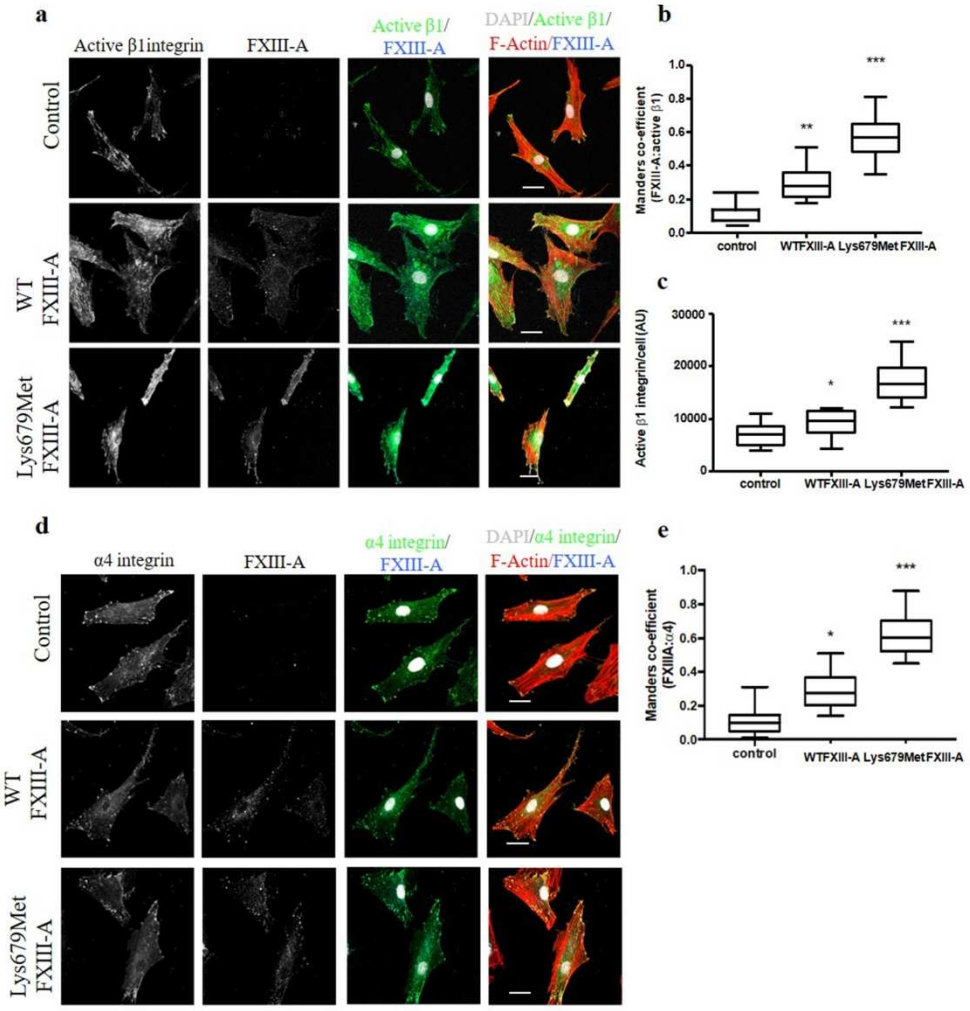

Figure 4: Co-localization of α4, β1 and FXIII-A on the cell surface suggests FXIII-A binds to α4β1 integrin Immunofluorescence staining and confocal microscopy of fixed, permeabilized NHDFs on coverslips after treatment with WT FXIII-A or Lys679Met FXIII-A for 2 hours before fixation. (a) Images show co-localization of active β1integrin and FXIII-A after treatment with either WT or mutant FXIII-A (scale bars 10um). (b) Manders overlap co-efficient analysis showing percentage overlap between FXIII-A and active β1integrin is greater for Lys679Met FXIII-A. (c) Level of Active β1 integrin intensity per cell is greater for Lys679Met FXIII-A. (d) Images show co-localization of α4 integrin and FXIII-A which is greater for Lys679Met FXIII-A compared to WT FXIII-A (scale bars 10um). (e) Manders overlap co-efficient analysis showing percentage overlap between FXIII-A and integrin is greater for Lys679Met FXIII-A. All experiments were done in triplicate. The data represent means +/- SD for three experiments* = $p<0.05$ vs control ** = $p<0.01$ vs control *** = $p<0.001$ vs control

188x196mm (300 x 300 DPI)

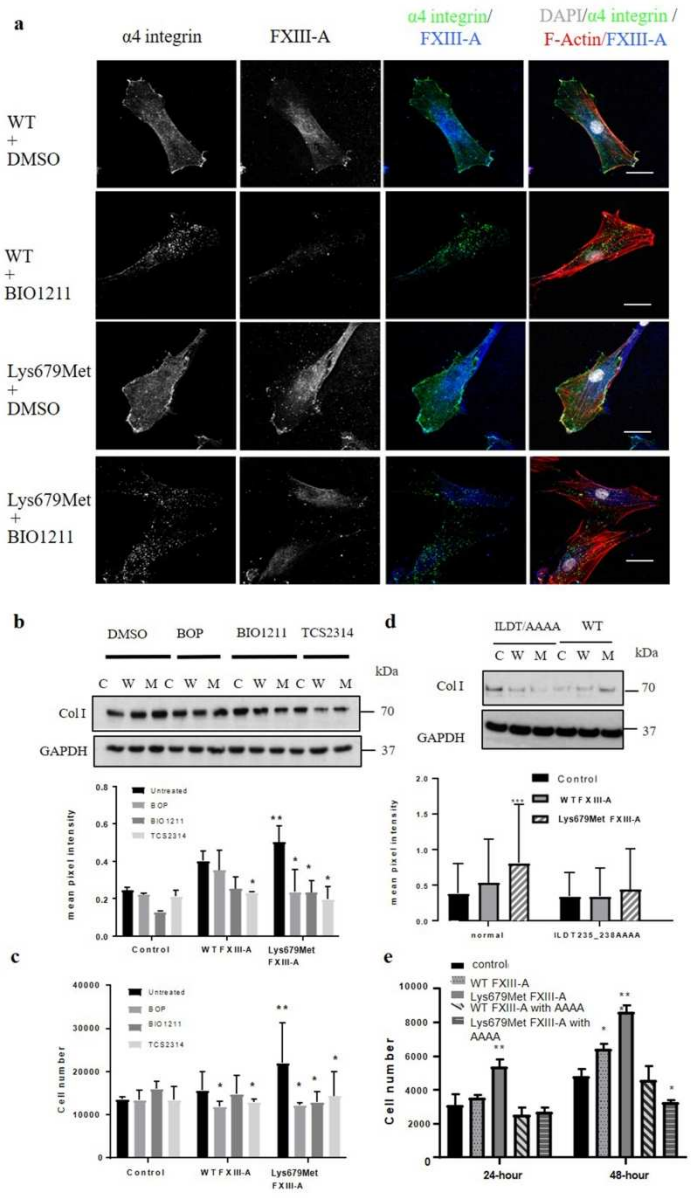

Figure 5: FXIII-A associates with α4β1integrin via the ILDT motif in FXIII-A. (a) NHDFs on coverslips were pre-treated with either DMSO (control) or BIO1211 (□4□1 integrin inhibitor) for 2 hours and then WT FXIII-A, Lys679Met FXIII-A and control conditioned media was added for 1 hour. Confocal images show that BIO1211 induces internalization of α4 integrin (small green dots); there is less FXIII-A binding for both WT and Lys679Met FXIII-A when cells are incubated with BIO1211 (scale bars 10um). (b) Western blots show reduction in collagen I expression after incubation with 3 different integrin inhibitors (BIO1211, BOP, TCS2314), particularly for cells treated with Lys679Met FXIII-A compared to WT FXIII-A. (c) Graph shows reduced cell proliferation rates following FXIII-A treatment (WT or Lys679Met) compared to control after incubation with the 3 integrin inhibitors at 48 hours. (d) Western blot shows reduction of Collagen I expression after 48-hour treatment with ILDT235_238AAAA FXIII-A. (e) Graph shows reduced cell proliferation rate after site-directed mutagenesis of ILDT motif of FXIII-A. These effects for (f) and (g) are common to the WT and Lys679Met FXIII-A but are more marked with Lys679Met FXIII-A. Experiments were performed in triplicate. The data show means +/- SD for three experiments*= p<0.05 vs control ** = p<0.01 vs control ***= p<0.001 vs control. C, W and M indicates control, wild type or mutant, respectively.

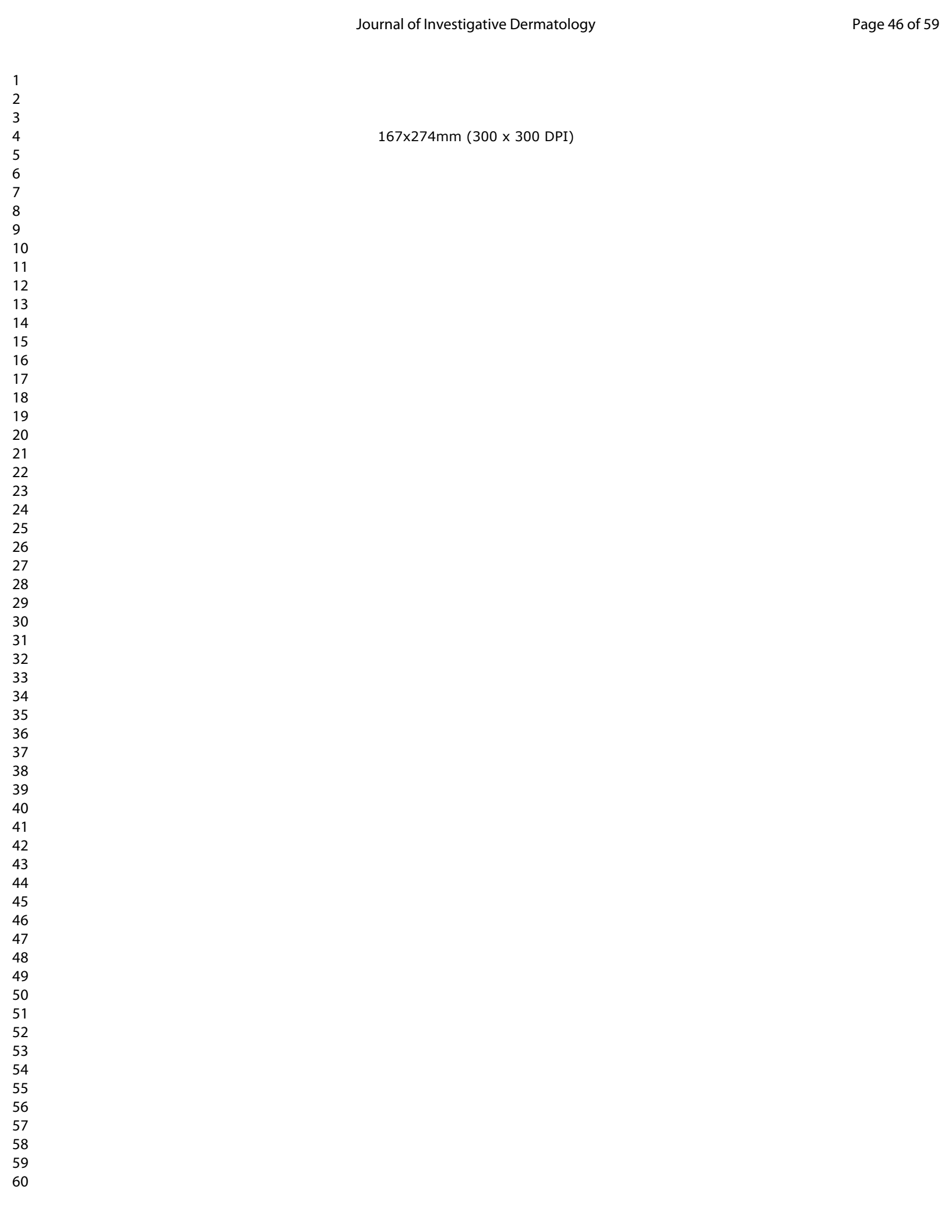
167x274mm (300 x 300 DPI)

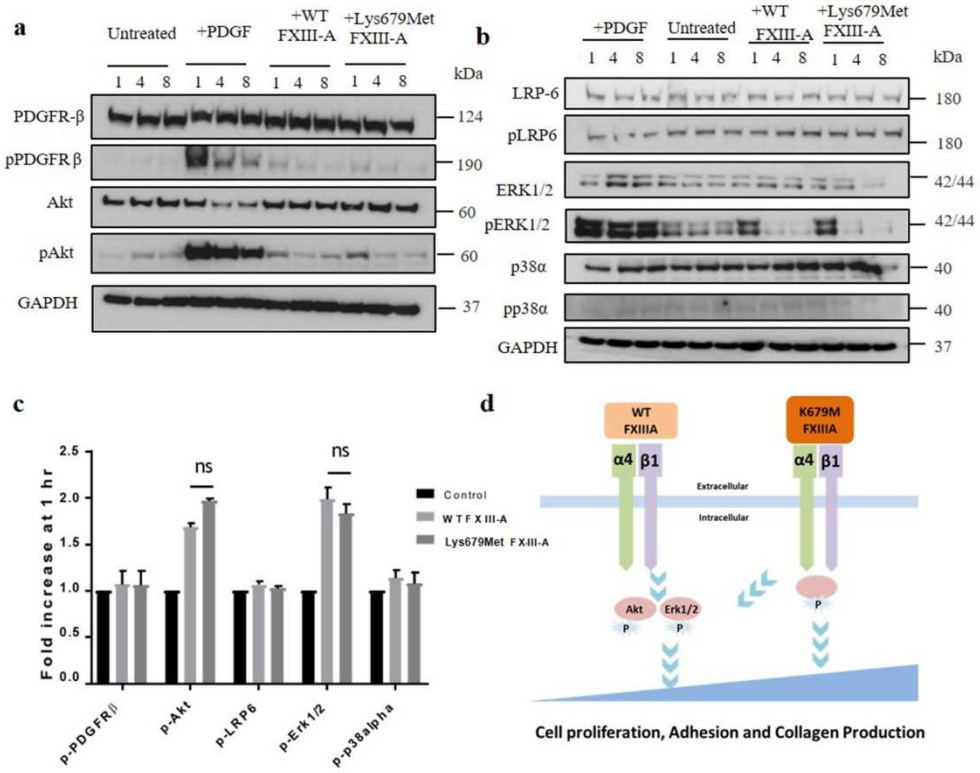

Figure 6: WT and Lys679Met FXIII-A both increase Akt and ERK1/2 activation. (a) NHDFs were treated with FXIII-A for 1, 4, or 8 hours with 2 nM PDGF-BB treatment as a positive control. Activation levels of PDGFR and Akt were determined by immunoblotting with antibodies to Tyr (p)-751-PDGFRβ and Ser(p)-473-Akt1. All samples were normalized for equal amount with glyceraldehyde-3-phosphate dehydrogenase (GAPDH). No activation was noted for p-PDGFR whereas both WT and Lys679Met FXIII-A showed transient increase in p-Akt signaling at 1 hour. (b) Activation level of LRP-6, ERK1/2 and p38α were determined by immunoblotting with antibodies to Ser (p)-1490-LRP6, Thr202 (p)/Thr204 (p)-p44/42MAPK (ERK1/2) and Thr (p)-180)/Tyr (p)-182-p38α. All samples were normalized for equal amounts with GAPDH. Both WT and Lys679Met FXIII-A showed transient increase in p-ERK1/2 signaling at 1 hour. (c) Phosphoproteins were quantified, averaged and expressed for NHDF cells treated with WT and Lys679Met FXIII-A as fold change over those of untreated cells. Both WT and Lys679Met FXIII-A showed similar ~two-fold increases in p-Akt and p-ERK1/2 compared to control. Shown are the means +/- SD for three experiments. (d) A proposed schematic figure for FXIII-A and α4β1 integrins association on the cell surface and downstream signaling. Lys679Met may lead to a conformational change in the protein which promotes α4 integrin binding (right panel). WT and Lys679Met FXIII-A after association with integrins activate Akt and Erk1/2 resulting in cell proliferation, adhesion and collagen production. However, the enhanced action of mutant FXIII-A on α4 integrin could initiate different signaling cascades which still remain to be determined.

181x151mm (300 x 300 DPI)

Supplementary information:

Coagulation Factor XIII-A Subunit Missense Mutation in the Pathobiology of Autosomal Dominant Multiple Dermatofibromas

Chavalit Supsrisunjai[1,2], Chao-Kai Hsu[1,3,4], Magdalene Michael[5], Cédric Duval[6], John Y. W. Lee[1], Hsing-San Yang[3], Hsin-Yu Huang[7], Thitiwat Chaikul[1], Alexandros Onoufriadis[1], Roberto Steiner[3], Robert A. S. Ariëns[4], Ofer Sarig[8], Eli Sprecher[8,9], Marina Schwartz-Eskin[8], Curt Samlaska[10], Michael A. Simpson[11], Eduardo Calonje[1, 12], Maddy Parsons[5*], John A. McGrath[1*]

Table S1: A summary of the stepwise filtering approach to identify potentially shared variant within two pedigrees

Pedigrees	Family 1 (Ukraine)			Family 2 (USA)				
	I-2	**II-2**	**III-1**	**II-1**	**II-3**	**II-2**	**III-2**	**II-5**
Total variants	26063	26327	26278	26006	26072	26061	26236	25818
Variants with MAF<0.01 in 1000 genomes, ESP, ExAC and 6000 control exomes	1098	870	849	911	893	952	936	881
Heterozygous variants	768	850	833	872	866	918	910	852
Heterozygous nonsynonymous, splice-site, or insertion/deletion variants	556	541	526	530	496	578	808	530
Shared variants among affected individuals	118			113				
Genes with variants that are shared between the two pedigrees	1 (*F13A1*)							

Table S2: A summary of the statistics of exome sequencing and coverage

	USA family					Ukraine family		
Case	**II-1**	**II-3**	**II-2**	**III-2**	**II-5**	**I-2**	**II-2**	**III-1**
Total reads	75853390	80748322	55446430	86094748	68319976	92053964	103018007	106717428
Reads uniquely mapped to +/- 150 bp of the target sequence	41705779 (54.98%)	43183922 (53.48%)	30637737 (55.26%)	47083150 (54.69%)	35757820 (52.34%)	71957989 (78.17%)	80224711 (77.87%)	83043872 (77.82%)
Reads uniquely mapped to target sequence	38934653 (51.33%)	40209995 (49.8%)	28501204 (51.4%)	43584762 (50.62%)	33379406 (48.86%)	65046797 (70.66%)	72451957 (70.33%)	74728981 (70.03%)
Mean_ Coverage (reads per position)	81.49	82.54	58.58	90.98	67.89	122.86	136.85	140.54
Target CCDS bases	33323618	33323618	33323618	33323618	33323618	33323618	33323618	33323618
CCDS bases with coverage > 1x	33113976 (99.37%)	33109377 (99.36%)	33140600 (99.45%)	33147115 (99.47%)	33067174 (99.23%)	32979225 (98.97%)	33001727 (99.03%)	33003929 (99.04%)
CCDS bases with coverage > 5x	32754189 (98.29%)	32721647 (98.19%)	32734490 (98.23%)	32792592 (98.41%)	32528456 (97.61%)	32753490 (98.29%)	32795207 (98.41%)	32789252 (98.4%)
CCDS bases with coverage > 10x	32241535 (96.75%)	32181220 (96.57%)	31910596 (95.76%)	32289315 (96.9%)	31807387 (95.45%)	32513166 (97.57%)	32600284 (97.83%)	32581726 (97.77%)
CCDS bases with coverage > 20x	31106314 (93.35%)	31018109 (93.08%)	29043630 (87.16%)	31234256 (93.73%)	30095747 (90.31%)	31826135 (95.51%)	32059438 (96.21%)	32031001 (96.12%)

*CCDS: Consensus coding sequence

Supplementary Methods and Results

F13A1 analysis in sporadic, non-familial dermatofibromas

We performed Sanger sequencing on 22 Taiwanese sporadic dermatofibroma samples and 28 in-house sporadic dermatofibromas sample to determine whether Lys679Met variants and other potential variants are present in any sporadic dermatofibromas. We also hypothesized that variants in the promoter region of *F13A1* might be associated with sporadic dermatofibroma. In order to determine single nucleotide polymorphisms (SNPs) in this area, Sanger sequencing was performed on *F13A1* gene and its promoter region. Regarding promoter region sequencing, we divided the promoter region (2400 bases) into 5 segments overlapping each other. The length of each segment is approximately 500 bases. Forward and reverse primers for each segment were designed by using an online tool (Primer 3) resulted in 5 pairs of primers (Supplementary table S6). A total of 50 sporadic dermatofibroma were sequenced for *F13A1* gene and 22 DNA samples for promoter region. AmpliTaq Gold® 360 Master Mix (Thermofisher) and PCR protocol were used as previously described. The ABI 3730 DNA Sequencher (SeqGen, CA, USA) was then used for analyzing the sequence. The allele frequencies of each SNPs were compared with population databases, i.e. 1000 Genome Project and ExAC Browser, where available. For unreported SNPs, we compared with 30, in-house Taiwanese control samples. All 50 sporadic dermatofibroma were successfully sequenced for a further SNPs analysis. The total of 3 variants in *F13A1* and 5 variants in promoter region were identified from Sanger sequencing (Supplementary table S3 and S4). None of these variants was statistically significant and different from the variants in the population database as compared by using Hardy-Weinberg equilibrium calculation and chi-square test (GraphPad Prism® version 8).

Table S3: Hardy-Weinberg equilibrium and chi-square test for analysis of SNPs in *F13A1* from sporadic dermatofibromas

Variant	Homozygous variant		Heterozygous variant		Wild type		P value (two-tailed)
	Observed #	Expected #	Observed #	Expected #	Observed #	Expected #	
rs5982 (c.1694C>T)	3	4.67	18	21.09	27	22.24	0.3561
rs5987 (c.1951G>A)	0	0.4	6	8.62	42	38.98	0.4889
rs5988 (c.1954G>C)	0	0.41	7	8.69	41	38.89	0.6517

Table S4: Hardy-Weinberg equilibrium and chi-square test for analysis of SNPs in *F13A1* promoter region from sporadic dermatofibromas

Variant	Homozygous variant		Heterozygote		Homozygous reference		P value (two-tailed)
	Observed #	Expected #	Observed #	Expected #	Observed #	Expected #	
rs1024231	9	8.715	9	9.996	3	2.289	0.8481
rs2815822	21	18.84	0	2.121	0	0.042	0.2995
rs1016925	0	0.42	5	6.867	13.71	16	0.5197
rs1267856	0	2.06	8	8.84	12	9.1	0.2161
rs1267855	2	2.74	7	9.44	11	7.82	0.3458

Exon	Forward Sequence	Tm (°C)	Reverse Sequence	Tm (°C)
Exon 2	ACATGCCTTTTCTGTTGTCTTC	56.5	CTGGACCCAGAGTGGTG	57.6
Exon 3	CAACCCTTGTTTTTCTTGTTC	54.0	CAATGCAACCCATGGTGTC	56.7
Exon 4	GGCTTGTGAAATCAACCTAAC	55.9	GAAAACTAAATGTCTGCCTC	53.2
Exon 5	ACAGTCTGGTTTGGTAATAG	53.2	GACAATAACAAATTTTAAGTGG	50.9
Exon 6	AGAGAATATTTTGCTTGCAGAG	54.7	GGCAAATGACAGGTGTAACAG	57.9
Exon 7	CCTTCTCACTTCTCACGGAC	59.4	AAGAAATTACTCAGTTGGATAC	52.8
Exon 8	GTGATGTGTTTAGCTGTGGT	55.3	GATTGAGTCTATCTTGTGGT	53.2
Exon 9	GGGATTACAGGCATGAGCCAC	61.8	AGATCAGCAATGAAGCAAGTTCC	58.9
Exon 10	TGGACAGAATTGGGAGATGAC	57.9	TGTGTTAAGAGGTTGGGGAG	57.3
Exon 11	ATGATGGCTAATGCTCTCCT	55.3	TTCTCTGGAACTCATCTCTG	55.3

Table S5 Primers for *F13A1*

Exon 12	CTGGTGGATTGTATTTTTGCC	55.9	ACAGCGAGTCTCACAAAGAAC	57.9
Exon 13	TGTGTGTGTTTTCTCCTACT	53.2	TTTGTCTCTGTTCCAGGATG	55.3
Exon 14	AGAGCAGAACGAGGTTTTATTTG	57.1	CACACAGAGAAAGCTTCCCAC	59.8
Exon 15	TCTTCCGAACCTCTCCTCTC	59.4	CCCTCTGCAGTCCTGTCTGG	63.5

Segment	position	Forward	Tm (°C)	Reverse	Tm (°C)
1	6:6321519 (-2678) – 6320920 (-2079)	GGCATGCACCTGTAGTTCC	59.1	AACCAGTTGCTGGGAGTACC	59.07
2	6:6321008 (-2344) – 6320456 (-1792)	AAACCCTCCCAGACCCTCT	59.9	GCAAGTGGAGCTGCCTGT	60.1
3	6:6320531 (-1867) – 6319949 (-1285)	ACCTCGGTTTCCTGGTTGA	60.5	TGAGAAATACCGAAGGTAGGC	58.3
4	6:6320031 (-1367) – 6319487 (-823)	CCCCTTAGCACTGTGTCTCC	59.7	GCAGGCACTGAGCCAGTTTA	61.5
5	6:6319570	CCCTTCATTTGGTCATTTGG	60.2	TGCATGTGCTGTATCTATGTTCA	59.3

Table S6 Primers for *F13A1* promoter region (6: 6,319,201 – 6,321,384:-1; 2 KB upstream from start codon of *F13A1*)

	(-906) – 6319039					
	Forward (-375)		Tm (°C)	Reverse		Tm (°C)
Lys679 Met FXIIIA	CCA ATG AAG **ATG** ATG TCC CGT GAA ATC CGG CCC AAC TCC ACC GTG		69.5	CAC GGT GGA GTT GGG CCG GAT TTC ACG GGA CAT **CAT** CTT CAT TGG		67.0
FXIIIA with AAAA	CTC TGT CCA TCA CAT ACA GGC AAG **CGG CCG CGG CGC** CAT CTT CAA ACT GAC CAT AGC T		93.5	AGC TAT GGT CAG TTT GAA GAT **GGC GCC GCG GCC G**CT TGC CTG TAT GTG ATG GAC AGA G		93.5

Table S7 Primers for site directed mutagenesis

Antibody	Product no.	Manufacturer	Concentration	Application
Human Integrin alpha 4/CD49d MAb (Clone 7.2R)	MAB1354	bioTechne	1:100 IF 1:1000 WB	IF, WB
Mouse monoclonal [12G10] to Integrin beta 1	NB100-63255	bioTechne	1:100 IF	IF
Rabbit polyclonal to FXIII-A	ab97636	Abcam	1:1000	WB
Sheep polyclonal to FXIII-A	ab 104559	Abcam	1:100	IF
Mouse monoclonal to Collagen I	sc-293182	Santacruz	1:200	WB
Mouse monoclonal to Collagen I	ab 90395	Abcam	1/2000	IF
Rabbit monoclonal [Y92] to PDGF Receptor beta	ab32570	Abcam	1:100 IF 1:5000 WB	IF, WB
Rabbit polyclonal to phosphor-PDGF-Receptor β(Tyr751)	3161	Cell Signaling Technology	1:1000	WB

Table S8 Primary and Secondary Antibodies

Polyclonal rabbit IgG to p38α	AF8691	bioTechne	0.5µg/mL	WB
Mouse monoclonal to human phospho-p38α	MAB8691	bioTechne	0.5µg/mL	WB
Rabbit polyclonal antibody to Akt	9272	Cell Signaling Technology	1:1000	WB
Antibody	Product no.	Manufacturer	Concentration	Application
Rabbit polyclonal antibody to pAkt(Ser473)	9271	Cell Signaling Technology	1:1000	WB
Rabbit IgG antibody to LRP-6	2560	Cell Signaling Technology	1:1000	WB
Rabbit polyclonal to phosphor-LRP6(Ser1490) antibody	2568	Cell Signaling Technology	1:1000	WB
Rabbit IgG antibody to p44/42 MAPK(ERK1/2) antibody	4695	Cell Signaling Technology	1:1000	WB
Rabbit IgG antibody to phosphor-p44/42 MAPK(ERK1/2)(Thr202/Tyr204) antibody	4370	Cell Signaling Technology	1:1000	WB

Rabbit polyclonal to fibronectin	ab2413	Abcam	1:100 IF 1:1000 WB	IF, WB
Rabbit polyclonal to GAPDH	ab9485	Abcam	1:2500	WB
Polyclonal Goat anti-rabbit Ig-HRP	P0448	Dako	1: 5000	WB
Polyclonal Goat anti-mouse Ig-HRP	P0447	Dako	1:2000	WB
Antibody	Product no.	Manufacturer	Concentration	Application
Mouse IgGκ binding protein-HRP	sc-516102	Santacruz	1: 1000	WB
Donkey Anti-Rabbit IgG H&L (Alexa Fluor 647)	ab150075	Abcam	1:200	IF
Donkey Anti-Sheep IgG H&L (Alexa Fluor; 568)	ab150177	Abcam	1:200	IF
Goat Anti-Mouse IgG H&L (Alexa Fluor 488)	ab150113	Abcam	1:200	IF

WB, western blot; IF, immunofluorescence; HRP, horseradish peroxidase

Supplementary Figures:

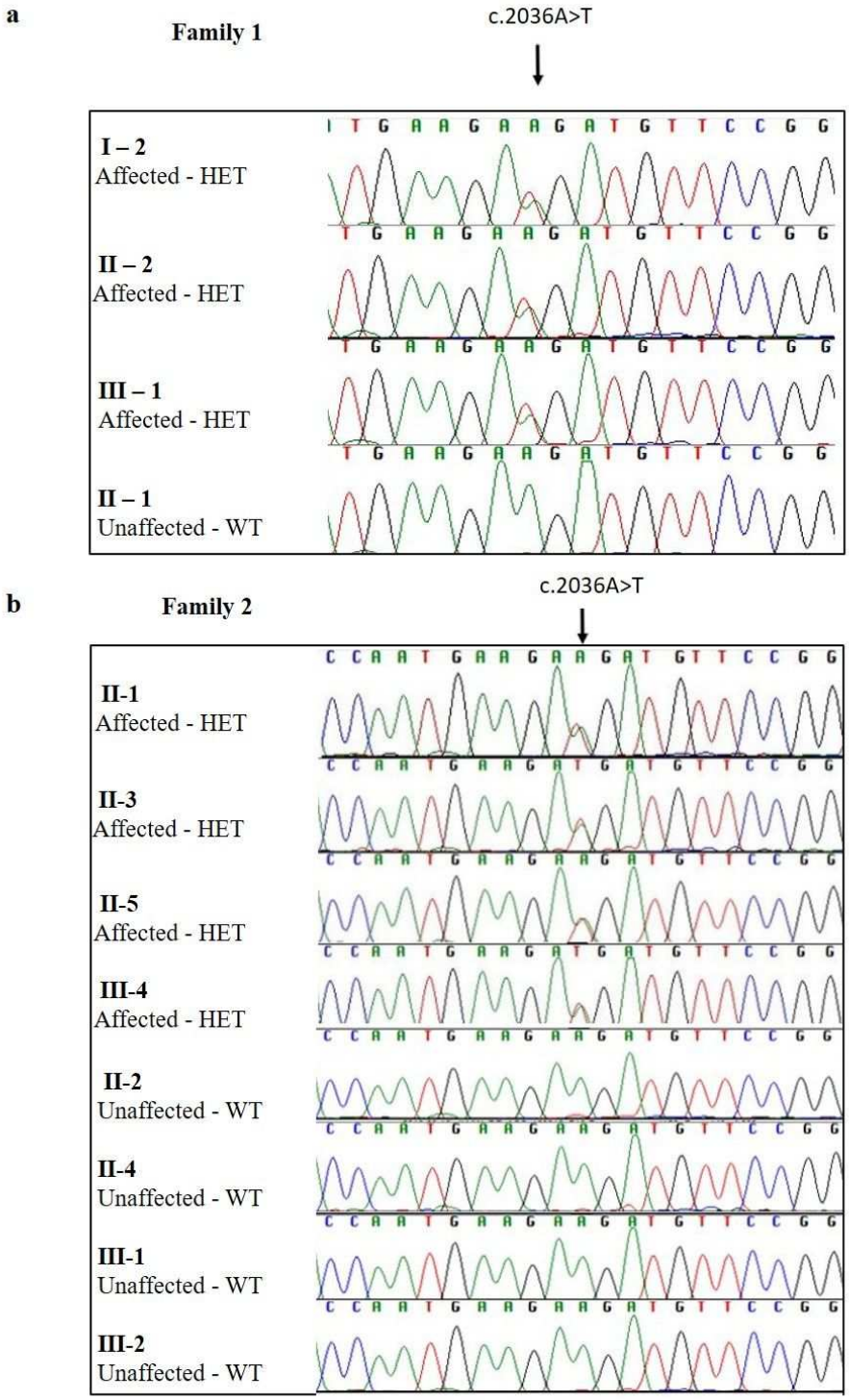

Figure S1. Chromatograms of *F13A1* gene reveals the heterozygous variant c.2036A>T (Lys679Met) in all affected subjects.

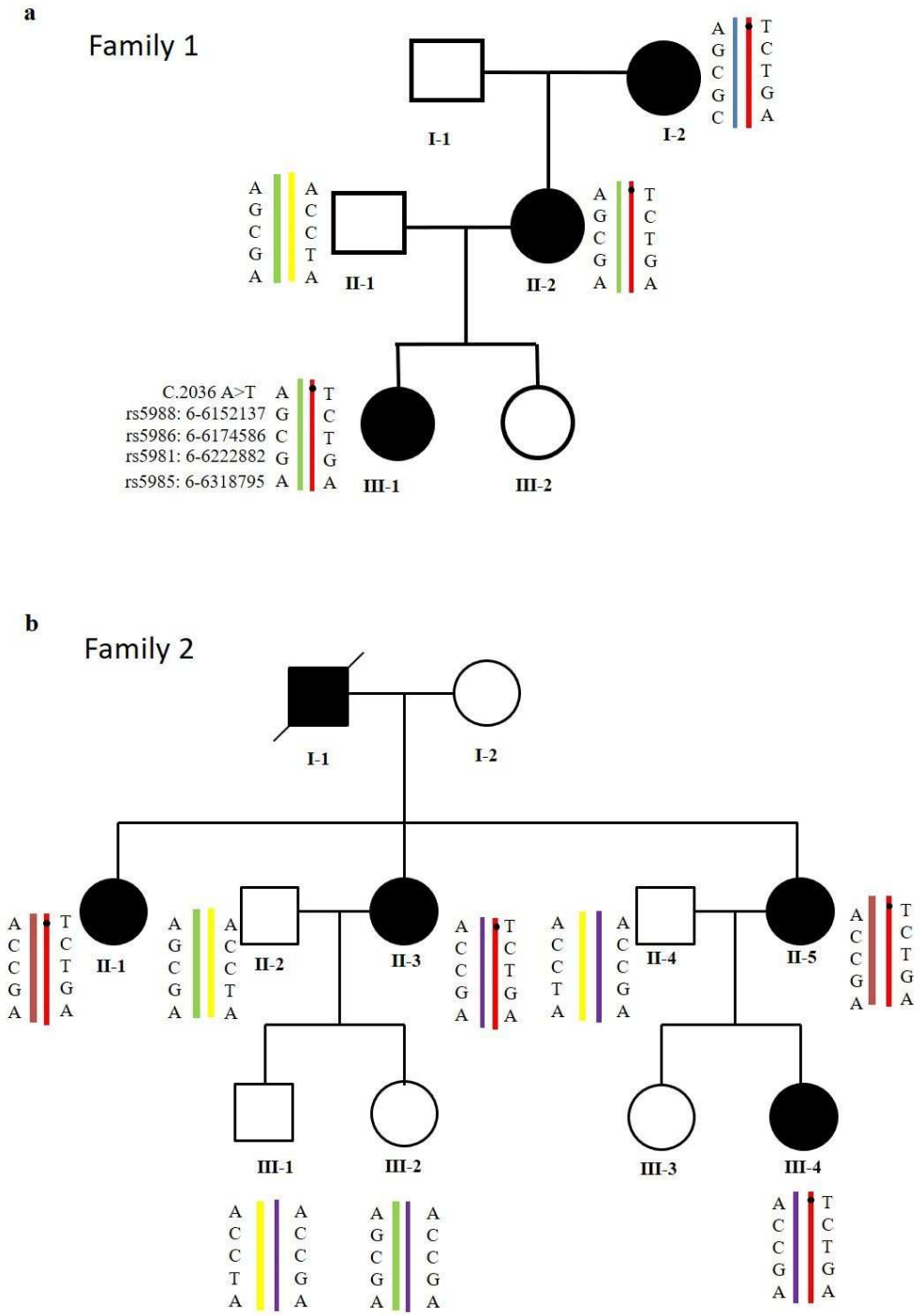

Figure S2. Haplotype analysis supports a common ancestral *F13A1* mutant allele in families 1 and 2. (a, b) SNP genotyping of two individuals in two families and their relatives with four highly polymorphic markers within *F13A1* shows that the individuals share the same haplogroup for the *F13A1* containing c.2036A>T (indicated by black spot). Each color bar represents a distinct haplotype.

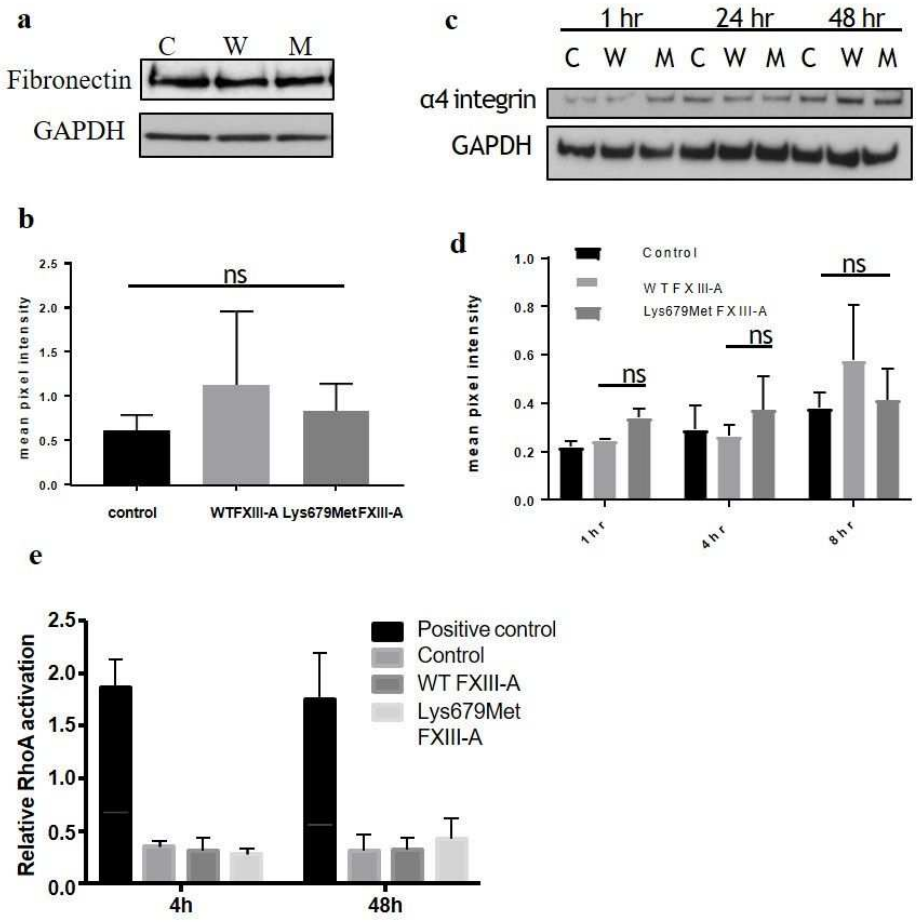

Figure S3: Levels of fibronectin and α4 integrin show no significant differences between treatments with either wild-type or mutant FXIII. (**a, b**) NHDFs were treated with FXIIIA for 48 hours with WT and Lys679Met FXIIIA; level of fibronectin was determined by immunoblotting with antibodies to Fibronectin. (**c, d**) NHDFs were treated with FXIIIA for 1, 24, 48 hours with WT and Lys679Met FXIIIA; level of α4 integrin was determined by immunoblotting. All samples were normalized for equal amounts with GAPDH. (**e**) NHDFs were treated with FXIIIA for 4 and 48 hours; level of RhoA was determined by GTPase-enzyme linked immunoabsorbent assay (G-LISA) Activation assays protocol (Cytoskeleton, Denver, CO). Shown are the means +/- SD for three experiments.